ROYAL SOCIETY
OF CHEMISTRY

PAPER

Check for updates

Single enantiomer chiral fullerenes enable interfacial toughening of perovskite solar cells†

Wenda Shi,‡[ab] Xin Wang, [ID] ‡[c] Ying Jiang,[d] Mengyao Zhang,[a] Sihan Du,[a] Qiang Zhuang,[a] Xueyan Hou,[e] Yuzhang Du, [ID] [a] Ruizhe Xing,[a] Jin Liang, [ID] [a] Zhen Yu,[a] Kailiang Ren,[a] Xiaoming Zhao, [ID] [d] T. John S. Dennis, [ID] [f] Xiangnan Sun,*[d] Matthew J. Fuchter [ID] *[bgh] and Jie Kong [ID] *[a]

The rapid advancements in perovskite solar cell (PSC) technologies are partly fueled by the integration of suitable electron transport layers (ETLs) to boost device performance. Despite continued improvements, inadequate robustness of the interface between the ETL and the perovskite limits PSC performance and operational stability. Fullerene derivatives are excellent ETLs in PSCs, though many commonly used fullerenes are used as mixtures of different isomers. The potential advantages of using single-isomer, single-enantiomer fullerenes in PSCs are poorly explored. In this study, we compare inverted PSCs incorporating the enantiomerically pure bis[60]phenyl-C_{61}-butyric acid methyl ester derivative (R,S, $^{f,s}A$) 49,59-bis[60]PCBM (*trans*-2) with a comparator enantiomer and with racemic material. Devices using this particular enantiomer exhibit significantly enhanced performance, achieving a power conversion efficiency (PCE) of 24.3%, as well as significantly enhanced ambient, thermal and operational stability. Overall, this study further highlights the promising role of single-isomer ETLs in advancing PSC technologies and provides early design rules of high-performance chiral fullerenes to enable future developments.

Introduction

Perovskite solar cells (PSCs) have attracted extensive research interest due to their cost-effectiveness, simple fabrication process and remarkable enhancement in certified power conversion efficiency (PCE),[1-3] reaching up to 26.7% for single junction PSCs,[4] and 33.9% for perovskite–silicon tandem solar cells as certified by the European Solar Test Installation. However, the soft lattice structure of perovskite crystals and the poor interfacial contact of PSCs has hindered their commercialization.[5-8] Compared to photovoltaic organic materials, halide perovskites are relatively less soft, generally exhibiting relatively poor mechanical properties in terms of strength, hardness, and toughness.[9-11] Poor mechanical properties will lead to poor contact at the interfaces between the perovskite layer and the adjacent charge transporting layers, such as electron/hole transport layers.[12-14] The mechanical stability of flexible PSCs and perovskite–silicon tandem solar cells is also poor, due to bending, deformation and thermal expansion, especially during the fabrication and working process.[15-19] These issues undermine the overall photovoltaic performance of PSCs. Considering that the interfaces are the weakest points in the devices, they exert a substantial influence on both the comprehensive mechanical integrity and operational stability of the cells. Therefore, augmenting interface toughness is a critical endeavour for the improvement and commercialization of PSC technologies.[20-23]

A number of methods have been explored to enhance the mechanical and operational durability of PSCs including the incorporation of additional interlayers, internal scaffolds, tailored additives, and enhancing crystal quality.[12-14,24-27] Despite the progress, there is still a significant need to identify strategies to resolve these issues and enhance the performance and long-term durability of PSCs. Improving interfacial contact between the electron/hole transport layers and the perovskite

aSchool of Chemistry and Chemical Engineering, Northwestern Polytechnical University, Xi'an, P. R. China. E-mail: kongjie@nwpu.edu.cn

bDepartment of Chemistry and Molecular Sciences Research Hub, Imperial College London, White City Campus, 82 Wood Lane, London W12 0BZ, UK

cSchool of Energy and Materials, Shanghai Polytechnic University, Shanghai, 201209, China

dInstitute for Frontier Science, Nanjing University of Aeronautics and Astronautics, Nanjing 210016, China. E-mail: xiangnan.sun@nuaa.edu.cn

eSchool of Physics, Liaoning University, Shenyang 110036, China

fAdvanced Materials Research Center, Department of Chemistry, School of Science, Xi'an Jiaotong-Liverpool University, Suzhou 215123, Jiangsu, China

gCentre for Processable Electronics, Imperial College London, South Kensington Campus, London SW7 2AZ, UK

hDepartment of Chemistry, Chemistry Research Laboratory, University of Oxford, 12 Mansfield Road, Oxford, OX1 3TA, UK. E-mail: matthew.fuchter@chem.ox.ac.uk

† Electronic supplementary information (ESI) available. See DOI: https://doi.org/10.1039/d4ta08040h

‡ The authors contributed equally to this work.

This journal is © The Royal Society of Chemistry 2025

J. Mater. Chem. A, 2025, **13**, 6089–6094 | **6089**

layer through structural tuning of the materials has been rarely studied, especially when considering the isomeric composition of the electron/hole transport layer.[28,29] We have previously separated both the regioisomers and enantiomers of bis[60]PCBM (bis(1-[3-(methoxycarbonyl)propyl]-1-phenyl)-[6,6]C_{62}) and demonstrated these to show advantages over the isomeric mixtures most commonly employed in fullerene-based materials.[28,30] In this study, we employed two such pure enantiomers from bis[60]PCBM (trans-2 and e) as two distinct electron transport layers (ETLs) for FAPbI$_3$ based PSCs. The sole structural difference between the two enantiomers used is the location of addends on the C_{60} cage (see Fig. 2A).[31–33] By calculating the absorption energy between the fullerene molecules and perovskite lattice, we found that the trans-2 enantiomers showed a much higher absorption energy of −0.38 eV in comparison to −0.08 eV for e enantiomers. The enhanced absorption energy boosts the PCE of the PSCs from 23.2% (e as the ETL) to 24.3% (trans-2 as the ETL), values which are also much higher than those achieved for racemic materials. Moreover, the optimized devices significantly enhanced ambient, thermal and operational stability. Under 1-sun illumination at 40 °C, devices with the trans-2A enantiomer ETL showed slower degradation, retaining 95% of their initial power conversion efficiency (PCE) after 3500 hours. In comparison, devices with the eA enantiomer ETL retained only 80% of the initial PCE. Under 85 °C conditions for 2000 hours, the eA-based device lost over 55% of PCE, while the trans-2A-based device had only a 20% PCE loss. This method provides a novel route to strengthen the interfacial toughness of PSCs and thus opens up an opportunity for high performance and durable PSCs.

Results and discussion

According to our previous purification methods for the e enantiomers (anti,S)16,17-bis[60]PCBM (eA) and (anti,R)16,17-bis[60]PCBM (eB),[28,30,31] we chose to isolate another pair of enantiomers for trans-2: (R,S, $^{f,s}A$)49,59-bis[60]PCBM (trans-2A) and (S,R, $^{f,s}C$)49,59-bis[60]PCBM (trans-2B). These enantiomers were isolated from the 10 pairs of enantiomers of bis[60]PCBM and used as novel ETLs for subsequent PSC fabrication. We have previously shown that the single enantiomer of the e isomer of bis[60]PCBM is a superior ETL when compared to the racemate. The superior performance of the pure enantiomer materials could be attributed to a higher electron extraction rate, improved electron mobility, and an altered molecular packing that suppresses ion immigration.[28] The molecular structures of the two trans-2 enantiomers are illustrated in Fig. 1A, which were isolated with a purity >99% through chiral peak-recycling HPLC following a five-stage purification process (Fig. 1B). The symmetric circular dichroism spectra of the two enantiomers exhibit a clear broadband chiroptical response spanning from 350 nm to 700 nm (Fig. 1C). The LUMO and
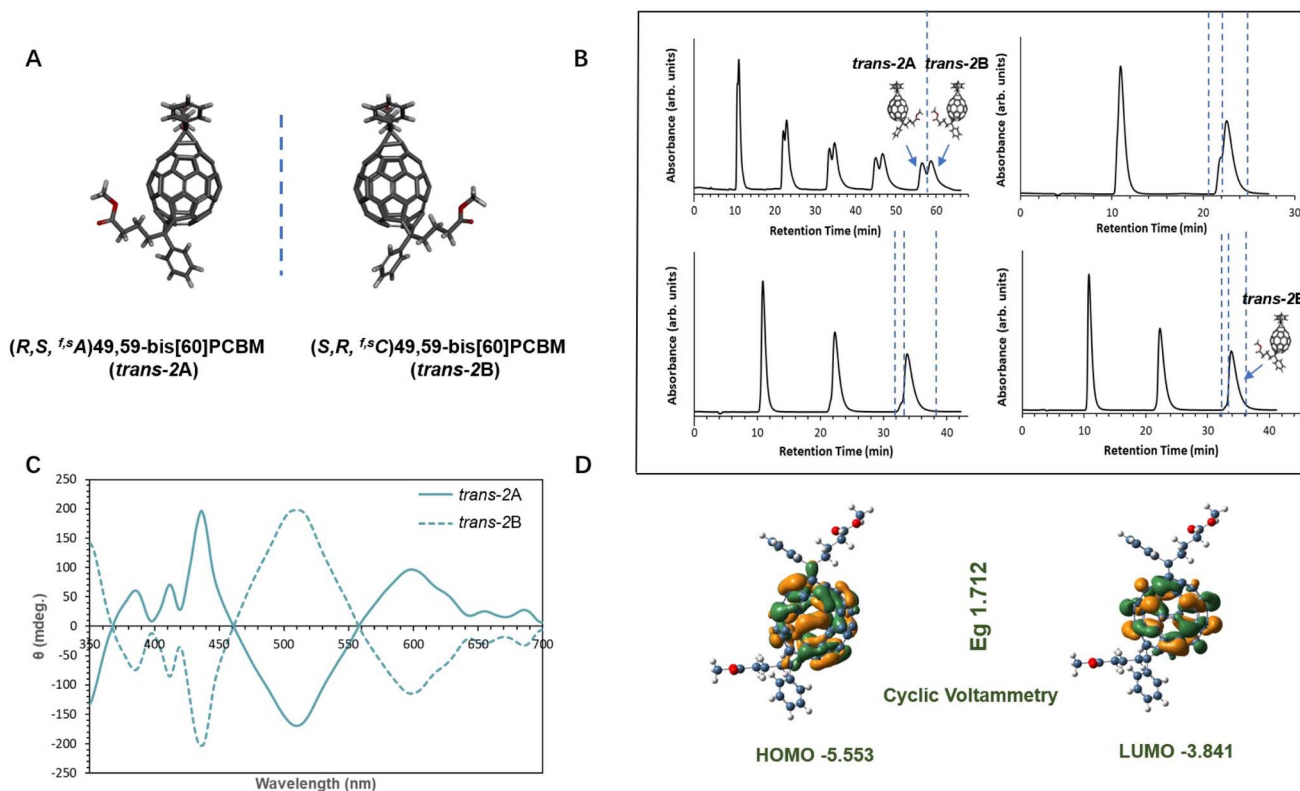

Fig. 1 Isolation and characterization of (R,S, $^{f,s}A$)49,59-bis[60]PCBM (trans-2A) and (S,R, $^{f,s}C$)49,59-bis[60]PCBM (trans-2B). (A) Molecular structures of each enantiomer. (B) Complete HPLC purification process for trans-2B, achieving purity exceeding 99% through peak-recycling HPLC. (C) Circular dichroism spectra of the enantiomers in toluene (~0.2 mg mL^{-1}). (D) HOMO, LUMO, and energy gap of the enantiomers, along with molecular geometries determined using DFT at the B3LYP/6-311G (2df,2pd) level of theory.

6090 | J. Mater. Chem. A, 2025, 13, 6089–6094

This journal is © The Royal Society of Chemistry 2025

HOMO for both the enantiomers and racemate are identical as would be expected, measured at −3.841 eV and −5.553 eV (Fig. 1D), respectively.

Density Functional Theory (DFT) calculations were carried out to investigate the adhesion between the *trans*-2A and eA molecules and the perovskite surface in terms of interfacial bonding (Fig. 2A). The absorption energy between the enantiomers and the FAPbI$_3$ lattice was used as a key indicator to evaluate the bonding strength between interfaces, as higher absorption energy typically indicates stronger intermolecular interactions resulting in more robust and stable interfacial bonding. The spin-polarized DFT calculations were performed using the Vienna *Ab initio* Simulation Package (VASP)[34] with the projector augmented wave (PAW) method,[35,36] with additional details provided in the ESI.† The interfacial interactions arise from the unsaturated bonds in the C$_{60}$ cage and oxygen atoms with Pb$^+$ and I$^-$ on the perovskite surface. The *trans*-2A molecule exhibited an absorption energy of −0.38 eV, approximately five times higher than the −0.08 eV absorption energy observed for eA (Fig. 2D). This significant difference in absorption energy may be attributed to the notably wider open angle configuration of the addends on *trans*-2A. In particular, one addend is positioned at the pole, while the other is located on the opposite hemisphere of the sphere. In contrast, for eA, one addend is situated at the pole, while the other is positioned equatorially. This wider open angle configuration promotes enhanced interfacial interactions through a larger contact area between the fullerene enantiomer and the FAPbI$_3$ lattice, which increases the absorption energy for *trans*-2A.[33]

Inverted perovskite solar devices were fabricated using single enantiomers *trans*-2A and *trans*-2B (Fig. 3A). For comparison, devices were also fabricated using PCBM, eA, and a 50 : 50 racemic mixture of *trans*-2 enantiomers. The key PSC parameters for the different ETLs are summarized in Table 1. Compared to the reference PCBM devices (using the common isomeric mixture), both the bis[60]PCBM racemic and enantiomer devices demonstrated improved performance in terms of open-circuit voltage (V_{OC}), short-circuit current density (J_{SC}), fill factor (FF), and overall power conversion efficiency (PCE). This already demonstrates the advantages posed by single regioisomer fullerene devices. Importantly, the *trans*-2 enantiomer devices achieved significantly enhanced PCE up to 24.3%, while the racemic *trans*-2 device only reached a PCE of 20.9% (Fig. 3B and E). Since both *trans*-2A and *trans*-2B showed similar photovoltaic performance, we chose to focus on *trans*-2A as a representative enantiomer for comparison with eA. As shown in Fig. 3C, F, and Table 1, the champion eA devices exhibited a V_{OC} of 1.15 V, J_{SC} of 25.2 mA cm^{-2}, FF of 0.80, and PCE of 23.2%. In contrast, the champion *trans*-2A devices demonstrated enhanced performance with a V_{OC} of 1.17 V, J_{SC} of 25.3 mA cm^{-2}, FF of 0.82, and a higher PCE of 24.3%. The significant improvement in V_{OC} can be attributed to its stronger intermolecular interactions provided by *trans*-2A, as evidenced by DFT results (Fig. 2D).[37] The J_{SC} values obtained from the *J–V* characteristics were consistent with those derived from the external quantum efficiency (EQE) spectrum (Fig. 3D). The stabilized power output was 22.7% for the eA devices and 23.9% for the *trans*-2A devices (Fig. 3E). These results suggest that a higher bonding strength resulting from the wider angle of the
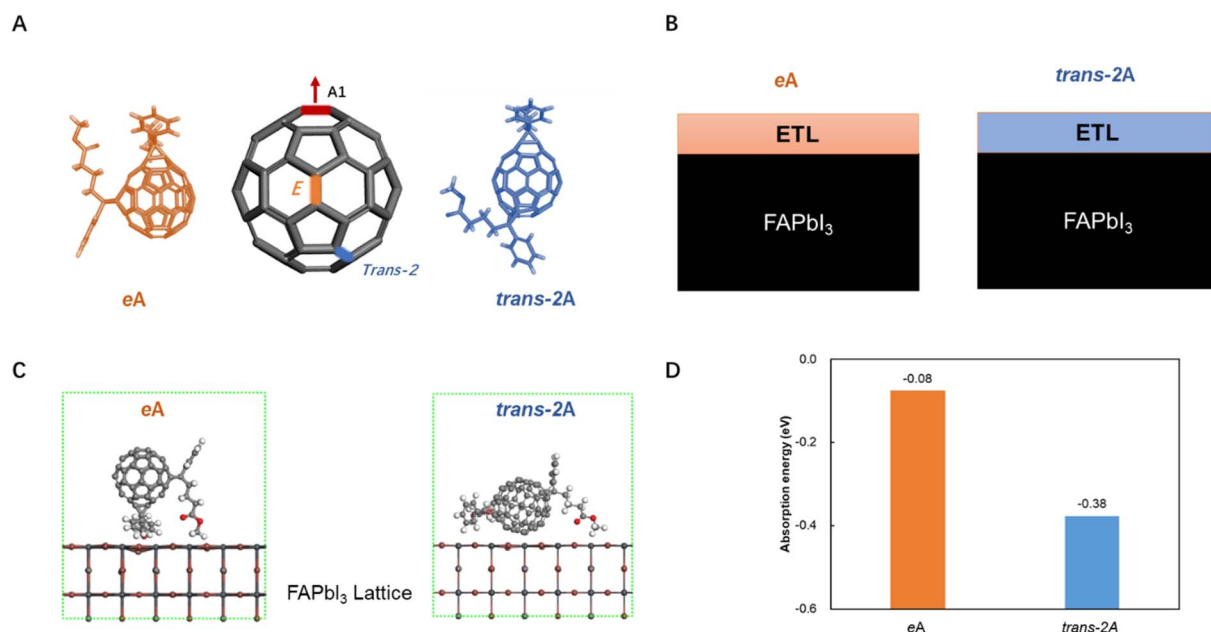

Fig. 2 Interfacial absorption energy between ETLs/perovskite interface. (A) Molecular structures of eA and *trans*-2A. (B) Schematic illustration of the bilayer structures of eA/*trans*-2A ETLs on the top of the perovskite, respectively. (C) Bonding between the FAPbI$_3$ (100) surfaces and *trans*-2A or eA. (D) Absorption energy of *trans*-2A/perovskite and eA/perovskite interface. The plane wave basis expansion had an energy cutoff of 400 eV, with partial occupancies handled by Gaussian smearing (0.2 eV width). Gamma point sampling was used for surface structure optimization, with convergence thresholds set at 10^{-4} eV for energy and 0.05 eV Å^{-1} for force. The bulk structure of FAPbI$_3$ was optimized with a 4 × 4 × 4 *k*-point, and the FAPbI$_3$ (100) surface contained 36 Pb, 36 C, and 108 I atoms.

This journal is © The Royal Society of Chemistry 2025

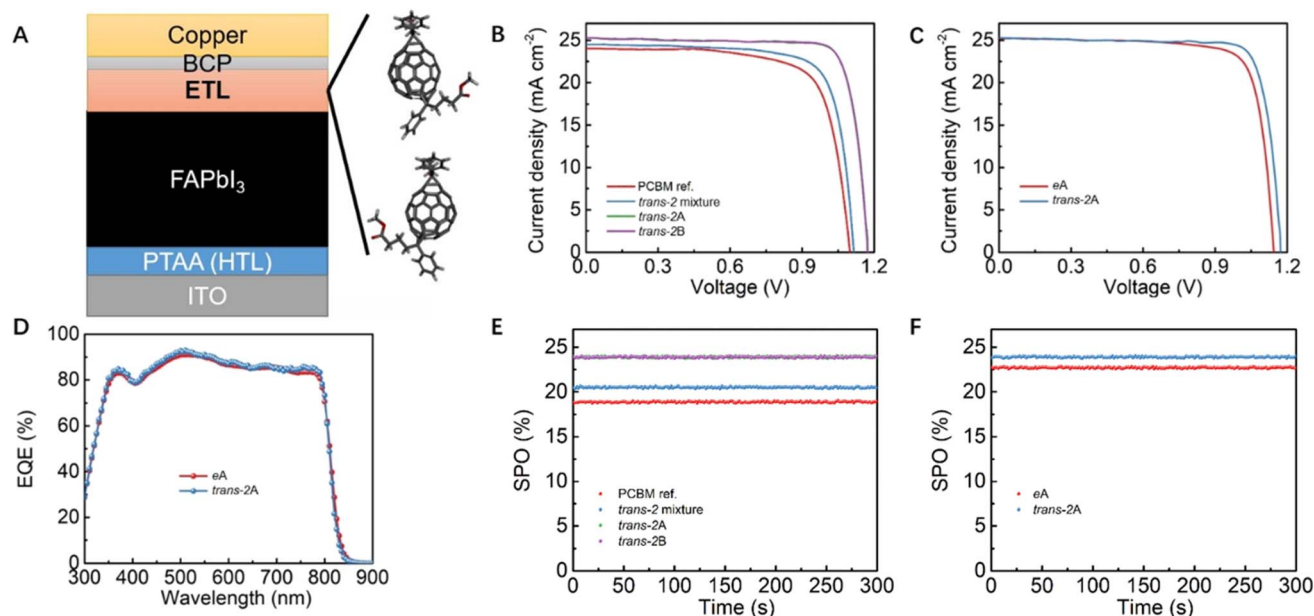*J. Mater. Chem. A*, 2025, **13**, 6089–6094 | **6091**

Fig. 3 PSC structure, photovoltaic characterization and device performance for *trans*-2A, *trans*-2B, eA, *trans*-2 racemic mixture and PCBM based ETLs. (A) Illustration of the inverted structure of PSC devices with ETLs atop the FAPbI$_3$ layer. (B) The *J–V* characteristics under reverse voltage scan of *trans*-2A, *trans*-2B, *trans*-2 racemic mixture and PCBM reference devices. (C) The *J–V* characteristics under reverse voltage scan of *trans*-2A *versus* eA devices. (D) External quantum efficiency (EQE) spectra of the eA *versus* *trans*-2A devices. (E and F) The stabilized power output of all the devices.

Table 1 PSC performance parameters. The values in brackets represent the average values and standard errors calculated from 20 devices

ETL	J_{SC} (mA cm^{-2})	J_{SC} from EQE	V_{OC} (V)	FF	PCE	SPO
PCBM ref.	24.0 (23.2 ± 0.4)	23.0	1.10 (1.08 ± 0.01)	0.74 (0.70 ± 0.02)	19.5% (17.8 ± 0.7)	18.9%
trans-2 Racemic mixture	24.5 (23.7 ± 0.5)	23.5	1.12 (1.09 ± 0.01)	0.76 (0.71 ± 0.02)	20.9% (19.6 ± 1.1)	20.5%
trans-2A	25.3 (24.6 ± 0.4)	24.3	1.17 (1.15 ± 0.01)	0.82 (0.78 ± 0.03)	24.3% (22.7 ± 0.9)	23.9%
trans-2B	25.3 (24.5 ± 0.5)	24.3	1.17 (1.15 ± 0.01)	0.82 (0.78 ± 0.03)	24.3% (22.9 ± 0.9)	23.9%
eA	25.2 (24.4 ± 0.5)	24.2	1.15 (1.13 ± 0.02)	0.80 (0.76 ± 0.03)	23.2% (21.9 ± 1.0)	22.7%

trans-2 addends improves the overall performance of PSCs, with single enantiomer materials having improved performance of the racemates.

The maximum power point (MPP) was evaluated to verify the operational stability of encapsulated devices under 1-sun illumination in a 40 °C ambient air environment. As shown in Fig. 4A, the device based on the *trans*-2A enantiomer ETL clearly exhibited much slower PCE decay. After approximately 3500 h continuous operation, 95% of the initial PCE was retained, demonstrating the long-term operational stability. For comparison, the PSC based on the eA enantiomer ETL only retains approximately 80% of the initial PCE. The stability achieved for the *trans*-2A enantiomer is among one of the highest stability values reported for PSCs to date.[38] Moreover, the MPP test in an 85 °C ambient air environment was also conducted for a duration of 2000 hours. The PSC based on the eA enantiomer ETL shows a typical rapid PCE degradation during the initial period of the test, with a loss of over 55% in PCE (Fig. 4C). The device based on the *trans*-2A enantiomer ETL,

however, exhibited only a 20% loss in PCE. Cross-sectional SEM images indicate that the enhanced operational stability of the *trans*-2A enantiomer may be attributed to the compact ETL/ perovskite interfacial contact. As shown in Fig. 4D, noticeable morphology degradation and an evident delamination phenomenon could be observed from the eA/perovskite interface. In contrast, the perovskite film displayed a compact and well-defined structure, and the ETL/perovskite interface is compact for the *trans*-2A/perovskite (Fig. 4B). This remarkable improvement in stability likely also stems from the enhanced interface contact resulting from the wider open angle of the two addends, which in turn contributes to a higher absorption energy at the interface. In addition, thermal analysis *via* TGA (Fig. S8†) and DSC (Fig. S9†)[33] demonstrates that both enantiomers exhibit high intrinsic thermal stability, with chemical decomposition temperatures around 390 °C and phase transition temperatures of 130 °C and 150 °C, respectively—far exceeding the operational temperature of the solar cells. These results indicate that the operational stability of the devices is
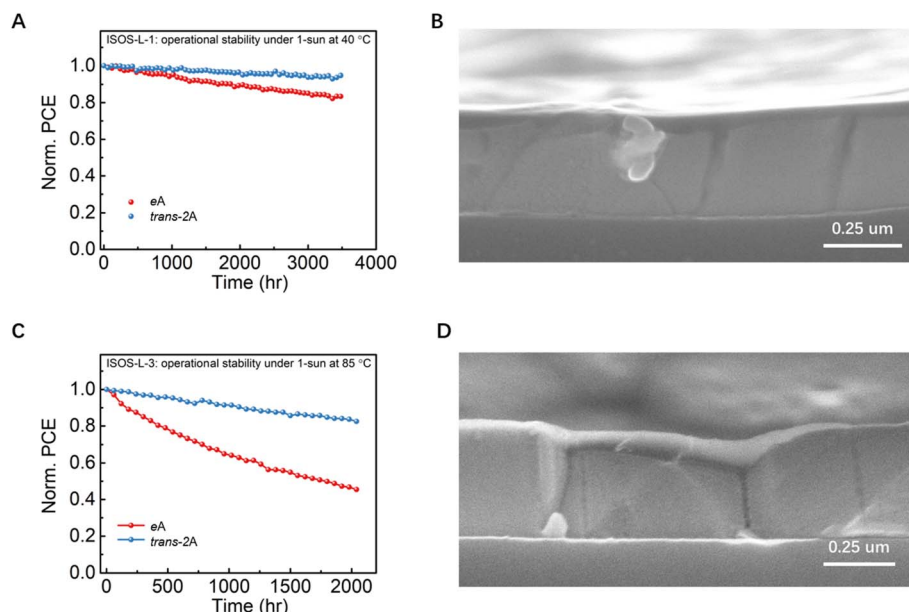
6092 | *J. Mater. Chem. A*, 2025, **13**, 6089–6094

This journal is © The Royal Society of Chemistry 2025

Fig. 4 Long-term stability of PSCs utilizing *trans*-2A/eA enantiomers as ETLs under varying operating conditions. (A) Maximum power point tracking (MPP) of encapsulated PSCs under simulated 1-sun illumination in 40 °C ambient air for about 3500 hours. (B) Cross-sectional SEM image of the *trans*-2A/perovskite bilayer tested over 3500 hours. (C) Maximum power point tracking (MPPT) of encapsulated PSCs under simulated 1-sun illumination in 85 °C ambient air over 2000 hours. (D) Cross-sectional SEM image of the eA/perovskite bilayer tested over 3500 hours.

primarily influenced by interfacial bonding and structural factors, rather than structure-dependent thermal properties.

Conclusion

We have successfully achieved fabrication of inverted PSCs employing a novel enantiomer of bis[60]PCBM as an ETL: *trans*-2. The resultant PSCs exhibit an enhanced efficiency of 24.3%, surpassing both racemic ETLs and enantiomeric ETLs from a close comparator chiral fullerene (e). Notably, we achieved one of the highest reported operational stabilities, retaining 95% of the initial efficiency after 3500 hours of operation. This underscores the success of our enantiomer-pure strategy, particularly the high interfacial bonding facilitated by specifically located addends with a relatively wide angle, leading to increased absorption energy. These results further advocate investigation into the fine structural tuning of ETLs for high stability PSCs, with single isomer and enantiomer fullerenes being excellent candidates for ETL materials.

Data availability

The datasets used in this study are available from the corresponding author upon request.

Author contributions

W. S., X. W. and Y. J. conceived and designed the experiments. W. S., X. W., M. Z., S. D., Q. Z., X. H., Y. D. and K. R. performed the experiments and acquired the data. W. S., R. Z., J. L., Z. Y., X.

Z. and T. J. D. analysed the data. X. S., M. J. F. and J. K., supervised the project.

Conflicts of interest

There are no conflicts to declare.

Acknowledgements

References

1 M. Noman, Z. Khan and S. T. Jan, *RSC Adv.*, 2024, **14**, 5085–5131.
2 Q. Jiang and K. Zhu, *Nat. Rev. Mater.*, 2024, **9**, 399–419.

This journal is © The Royal Society of Chemistry 2025

J. Mater. Chem. A, 2025, **13**, 6089–6094 | **6093**

3 X. Zhao, T. Liu and Y. L. Loo, *Adv. Mater.*, 2022, **34**, 2105849.

4 M. A. Green, E. D. Dunlop, M. Yoshita, N. Kopidakis, K. Bothe, G. Siefer, D. Hinken, M. Rauer, J. Hohl-Ebinger and X. Hao, *Prog. Photovolt.: Res. Appl.*, 2024, **32**, 425–441.

5 Y. Li, H. Xie, E. L. Lim, A. Hagfeldt and D. Bi, *Adv. Energy Mater.*, 2022, **12**, 2102730.

6 C. Luo, G. Zheng, F. Gao, X. Wang, C. Zhan, X. Gao and Q. Zhao, *Nat. Photonics*, 2023, **17**, 856–864.

7 Y. Wang, T. Wu, J. Barbaud, W. Kong, D. Cui, H. Chen, X. Yang and L. Han, *Science*, 2019, **365**, 687–691.

8 J. Ali, Y. Li, P. Gao, T. Hao, J. Song, Q. Zhang, L. Zhu, J. Wang, W. Feng, H. Hu and F. Liu, *Nanoscale*, 2020, **12**, 5719–5745.

9 G. Yuan, W. Xie, Q. Song, S. Ma, Y. Ma, C. Shi, M. Xiao, F. Pei, X. Niu, Y. Zhang, J. Dou, C. Zhu, Y. Bai, Y. Wu, H. Wang, Q. Fan and Q. Chen, *Adv. Mater.*, 2023, **35**, 2211257.

10 X. Zhao, L. Tian, T. Liu, H. Liu, S. Wang, X. Li, O. Fenwick, S. Lei and W. Hu, *J. Mater. Chem. A*, 2019, **7**, 1509–1518.

11 N. Rolston, A. D. Printz, J. M. Tracy, H. C. Weerasinghe, D. Vak, L. J. Haur, A. Priyadarshi, N. Mathews, D. J. Slotcavage and M. D. McGehee, *Adv. Energy Mater.*, 2018, **8**, 1702116.

12 X. Zhao, C. Yao, K. Gu, T. Liu, Y. Xia and Y.-L. Loo, *Energy Environ. Sci.*, 2020, **13**, 4334–4343.

13 T. Liu, X. Zhao, X. Zhong, Q. C. Burlingame, A. Kahn and Y.-L. Loo, *ACS Energy Lett.*, 2022, **7**, 3531–3538.

14 X. Zhao, T. Liu, Q. C. Burlingame, T. Liu, R. Holley III, G. Cheng, N. Yao, F. Gao and Y.-L. Loo, *Science*, 2022, **377**, 307–310.

15 I. K. Popoola, M. A. Gondal and T. F. Qahtan, *Renewable Sustainable Energy Rev.*, 2018, **82**, 3127–3151.

16 Q. Dong, M. Chen, Y. Liu, F. T. Eickemeyer, W. Zhao, Z. Dai, Y. Yin, C. Jiang, J. Feng and S. Jin, *Joule*, 2021, **5**, 1587–1601.

17 M. Li, Y. G. Yang, Z. K. Wang, T. Kang, Q. Wang, S. H. Turren-Cruz, X. Y. Gao, C. S. Hsu, L. S. Liao and A. Abate, *Adv. Mater.*, 2019, **31**, 1901519.

18 L. Duan, D. Walter, N. Chang, J. Bullock, D. Kang, S. P. Phang, K. Weber, T. White, D. Macdonald and K. Catchpole, *Nat. Rev. Mater.*, 2023, **8**, 261–281.

19 B. Chen, N. Ren, Y. Li, L. Yan, S. Mazumdar, Y. Zhao and X. Zhang, *Adv. Energy Mater.*, 2022, **12**, 2003628.

20 Z. Dai, S. K. Yadavalli, M. Chen, A. Abbaspourtamijani, Y. Qi and N. P. Padture, *Science*, 2021, **372**, 618–622.

21 Z. Dai, S. Li, X. Liu, M. Chen, C. E. Athanasiou, B. W. Sheldon, H. Gao, P. Guo and N. P. Padture, *Adv. Mater.*, 2022, **34**, 2205301.

22 I. S. Yang, Z. Dai, A. Ranka, D. Chen, K. Zhu, J. J. Berry, P. Guo and N. P. Padture, *Adv. Mater.*, 2024, **36**, 2308819.

23 X. Leng, Y. Zheng, J. He, B. Shen, H. Wang, Q. Li, X. Liu, M. Lin, Y. Shi and Z. Wei, *Energy Environ. Sci.*, 2024, **17**, 4295–4303.

24 X. Zhao, M. L. Ball, A. Kakekhani, T. Liu, A. M. Rappe and Y.-L. Loo, *Nat. Commun.*, 2022, **13**, 3970.

25 X. Zhao, T. Liu, A. B. Kaplan, C. Yao and Y.-L. Loo, *Nano Lett.*, 2020, **20**, 8880–8889.

26 Y. Zhang and N. G. Park, *Adv. Funct. Mater.*, 2023, **33**, 2308577.

27 X. Zhong, X. Ni, A. Kaplan, X. Zhao, M. Ivancevic, M. L. Ball, Z. Xu, H. Li, B. P. Rand and Y. L. Loo, *Adv. Energy Mater.*, 2024, **14**, 2304345.

28 W. Shi, Q. Zhuang, R. Zhou, X. Hou, X. Zhao, J. Kong and M. J. Fuchter, *Adv. Energy Mater.*, 2023, **13**, 2300054.

29 F. Zhang, W. Shi, J. Luo, N. Pellet, C. Yi, X. Li, X. Zhao, T. J. S. Dennis, X. Li, S. Wang, Y. Xiao, S. M. Zakeeruddin, D. Bi and M. Grätzel, *Adv. Mater.*, 2017, **29**, 1606806.

30 W. Shi, F. Salerno, M. D. Ward, A. Santana-Bonilla, J. Wade, X. Hou, T. Liu, T. J. S. Dennis, A. J. Campbell, K. E. Jelfs and M. J. Fuchter, *Adv. Mater.*, 2021, **33**, 2004115.

31 W. Shi, X. Hou, T. Liu, X. Zhao, A. B. Sieval, J. C. Hummelen and T. J. S. Dennis, *Chem. Commun.*, 2017, **53**, 975–978.

32 X. Hou, A. J. Clarke, M. Azzouzi, J. Yan, F. Eisner, X. Shi, M. F. Wyatt, T. J. S. Dennis, Z. Li and J. Nelson, *J. Mater. Chem. C*, 2022, **10**, 7875–7885.

33 X. Hou, J. F. Coker, J. Yan, X. Shi, M. Azzouzi, F. D. Eisner, J. D. McGettrick, S. M. Tuladhar, I. Abrahams, J. M. Frost, Z. Li, T. J. S. Dennis and J. Nelson, *Chem. Mater.*, 2024, **36**, 425–438.

34 G. Kresse and J. Furthmüller, *Comput. Mater. Sci.*, 1996, **6**, 15–50.

35 P. E. Blochl, *Phys. Rev. B:Condens. Matter Mater. Phys.*, 1994, **50**, 17953–17979.

36 J. P. Perdew, J. A. Chevary, S. H. Vosko, K. A. Jackson, M. R. Pederson, D. J. Singh and C. Fiolhais, *Phys. Rev. B:Condens. Matter Mater. Phys.*, 1992, **46**, 6671–6687.

37 J. Y. Qi, R. Q. Wang, X. Chen, F. Wu, W. Shen, M. Li, R. X. He and X. R. Liu, *J. Mater. Chem. A*, 2024, **12**, 4067–4076.

38 H. Zhu, S. Teale, M. N. Lintangpradipto, S. Mahesh, B. Chen, M. D. McGehee, E. H. Sargent and O. M. Bakr, *Nat. Rev. Mater.*, 2023, **8**, 569–586.

6094 | *J. Mater. Chem. A*, 2025, **13**, 6089–6094

This journal is © The Royal Society of Chemistry 2025